Performance and mass transport in open metallic element architecture fuel cells at ultra-high current density

A.K. Srouji [a], L.J. Zheng [b], R. Dross [c], A. Turhan [d], M.M. Mench [d,e,*]

[a] Department of Energy and Mineral Engineering, The Pennsylvania State University, University Park, PA 16801, USA
[b] Department of Mechanical and Nuclear Engineering, The Pennsylvania State University, University Park, PA 16801, USA
[c] Nuvera Fuel Cells Inc., Billerica, MA 01821, USA
[d] Electrochemical Energy Storage and Conversion Laboratory, Department of Mechanical, Aerospace and Biomedical Engineering, University of Tennessee, Knoxville, TN 37996, USA
[e] Energy and Transportation Science Division, Oak Ridge National Laboratory, Oak Ridge, TN 37831, USA

HIGHLIGHTS

► Novel flow field made of an open metallic element enabling enhanced mass transport.
► Flow field enables ultra-high current density i.e.: 3 A cm^{-2}.
► Fundamental comparison with conventional parallel channel/land design.
► Investigation of effect of enhanced mass transport.
► Enhanced reactant transport means enhanced water removal leading to dry out.

ARTICLE INFO

ABSTRACT

Performance and mass transport of a polymer electrolyte fuel cell (PEFC) with an open metallic element (OME) flow field architecture were analyzed in comparison to a conventional parallel channel/land (C/L) fuel cell, using low humidity at the anode and dry oxidant at the cathode. Under identical conditions the OME cell was able to operate at a current density of 3 A cm^{-2}, recording a peak power of 1.2 W cm^{-2}, compared to 0.9 W cm^{-2} using a parallel cell. Area specific resistance (ASR) was lower for the OME cell as a result of more uniform compression and reduced contact resistance. Electrochemical impedance spectroscopy (EIS) revealed great improvement in mass transport compared to a parallel C/L cell. A heliox mixture at the cathode of both cells revealed improved mass transport for the parallel cell, but revealed no oxygen gas phase transport limitation at high current densities for the OME architecture. In fact, it was shown that with an OME architecture, limitation at ultra-high current density results from dehydration at the anode and not reactant mass transport. This also indicates that ionomer film resistances at the electrode do not preclude operation at extremely high currents.

© 2012 Elsevier B.V. All rights reserved.

1. Introduction

The polymer electrolyte fuel cell (PEFC) is a possible alternative to the internal combustion engine for many applications. In the context of clean and sustainable energy, the PEFC is a zero emission technology when using hydrogen gas produced from renewable sources. The majority of automotive manufacturers are engaging in PEFC research and development, and numerous prototype vehicles have already been developed and demonstrated competent performance and range. Market entry is planned in 2015, but reduction in cost below the state-of-the-art system price of 46 \$ kW^{-1} is still needed [1].

Reactant gases in a fuel cell are distributed over the gas diffusion media (DM) through a flow field, before diffusing to the reaction sites. For functional requirements, the design of a flow field must achieve adequate reactant gas distribution over their respective electrodes, provide pathways for water evacuation from the cell, translate compression from the end plates/bipolar plates to the soft materials layered within, and provide necessary electrical conduction and heat transfer.

A variety of flow field designs are well developed, including parallel, serpentine, and interdigitated (e.g. [2–9]). It is important to note that even though different flow field layouts have been developed, they are generally based on a conventional alternating channel/land distribution. Parallel flow fields suffer from uneven gas flow supply and water droplet accumulation, which can result in poor performance at high current or wet conditions. Neutron imaging utilized to quantify liquid water accumulation and distribution in a PEFC showed that locations under lands have restricted mass transport and are preferential liquid storage sites, even in dryer operating conditions [10]. It was also shown that decreasing the land-to-channel ratio is advantageous in decreasing the water stored in the cell, but could be a drawback when operating in low humidity conditions [11]. Another neutron study revealed that the liquid storage in the gas diffusion layer increased with larger lands [12]. Larger lands create increased distance for transport of products from the electrode, and also add a shadowing effect for reactants diffusing to the electrode. A serpentine layout suffers from relatively higher pressure drop and concentration gradients since the flow path is relatively long. Liquid water has also been shown to accumulate in turns and switchbacks [13,14], which can harm performance, stability, and durability. The presence of lands introduces a drawback since reactant gas must diffuse under the lands to reach the electrode. At high current density, the land width was found to be the dominant factor for performance. At the same time, large channel spans cause additional ohmic resistance [15], and increase DM intrusion in the channel [16,17]. The under-compressed DM surface below the channel makes less contact with the catalyst layer [18]. It is also shown that water in low compression interfaces is prone to ice lens formation during operation or storage at subfreezing temperatures, which ultimately causes mechanical damage to the soft materials [19]. Conventional channel/land configurations have also been developed with porous carbon material that acts as an integrated passive wick that removes excess water from the channels and DM [20–22].

The motivation of this study is to understand factors which limit ultra-high current density in fuel cells, so that reduced system cost can ultimately be achieved through higher power density stacks. To help achieve this, a single cell with open metallic element, conceived and designed by Nuvera Fuel Cells (Billerica, MA), with a flow field capable of dramatically increasing limiting current density compared to conventional design, was tested. The elimination of lands in the flow field is the unique concept behind this architecture. A conventional parallel land/channel fuel cell was used as a comparative reference, in order to better understand the increase in power density observed with the open metallic element design. A set of operating conditions of particular interest to the automotive industry were used in order to operate both cells as shown in Table 1. The results of this study provide a comparison between conventional parallel C/L design and an open metallic element for the first time in literature, and show different origins of performance limitation of the two designs. The experimental work also provides validation data for simultaneous modeling efforts of the open metallic element design [23].

2. Experimental

Two single cells were used in this comparative study. The first cell has a conventional C/L flow field in parallel configuration as shown in Fig. 1(a), with an active area of 25 cm^2. The second cell has an open metallic element acting as flow field and an active area measuring 50 cm^2, as seen in Fig. 1(b). Both cells' flow fields have the same length in the direction of the flow, making the comparison of two different sized cells possible. The anode and cathode reactant flows were operated in a counter-flow arrangement.

Table 1
Fuel cell automotive operating conditions.

Gas	Anode		Cathode	
	Hydrogen		Air or heliox (21% O$_2$, Bal. He)	
Relative humidity	53%		Dry (humidifier bypassed)	
Current density (A cm^{-2})	Stoichiometry	Inlet pressure (kPa, absolute)	Stoichiometry	Inlet pressure (kPa, absolute)
0.25	2	118	1.6	118
0.5	2	129	1.7	129
1	2	152	1.8	152
1.5	2	175	1.9	175
2	2	180	2	180
2.5	2	180	2	180
3.0	2	180	2	180

All experiments were conducted using commercial type membrane electrolyte assembly (MEA) composed of an 18 μm (dry) membrane with a catalyst loading of 0.15 mg Pt. cm^{-2} at the anode and 0.4 mg Pt. cm^{-2} at the cathode. The diffusion media (DM) used on both electrodes are Sigracet 25BC by SGL Group (Wiesbaden, Germany), which have a 5% PTFE content and a micro porous layer (MPL) with 23% PTFE content.

An Arbin Instruments (College Station, TX) fuel cell testing station was used for all experiments. The gases were humidified using a standalone membrane-type humidification system from Fuel Cell Technologies Inc. (Albuquerque, NM). Gas inlet pressure was controlled with a backpressure unit from Scribner Associates Inc. (Southern Pine, NC).

Electrochemical impedance spectroscopy (EIS) was performed using a Zahner IM6ex with an external EL300 load, by Zahner Elektrik (Kronach, Germany). The frequency was swept from 100 mHz to 5 kHz using a 20 mV amplitude signal.

Two dew point temperature sensors by Vaisala Inc. (Helsinki, Finland) were used to measure the dew point temperatures of the gases exiting the anode and cathode of the OME cell, in order to compute the net water drag coefficient.

The cells temperatures were maintained at 60 °C with high flow rate coolant (DI water) from a re-circulating bath for all experiments. Table 1 summarizes the test protocol employed in all experiments unless otherwise specified. The anode side was fed with hydrogen gas at 53% inlet relative humidity (RH), with a constant stoichiometry of 2. The cathode side was fed with dry air or heliox at a stoichiometry increasing from 1.6 to 2 with 0.1 increments as current is increased from 0.25 to 2 A cm^{-2}. The stoichiometry remained 2 for any current density above 2 A cm^{-2}. The same inlet pressure was set on both sides of the cell by applying backpressure. Inlet pressure was throttled from 118 kPa to 180 kPa (absolute pressure) with increasing current density up to 2 A cm^{-2}. After 2 A cm^{-2} inlet pressure remained constant at 180 kPa. The cell was operated in galvanostatic mode. Each point on the polarization curves shown corresponds to a 45 min operation average.

3. Results and discussion

3.1. Performance comparison of open metallic element (OME) and conventional design

The performance curves obtained using the parallel C/L flow field architecture with air at the cathode, are shown in Fig. 2, and are well known. The low pressure (atmospheric pressure at cell outlets) curve represents an ideal for future automotive conditions where parasitic losses are minimized. However, with the existing
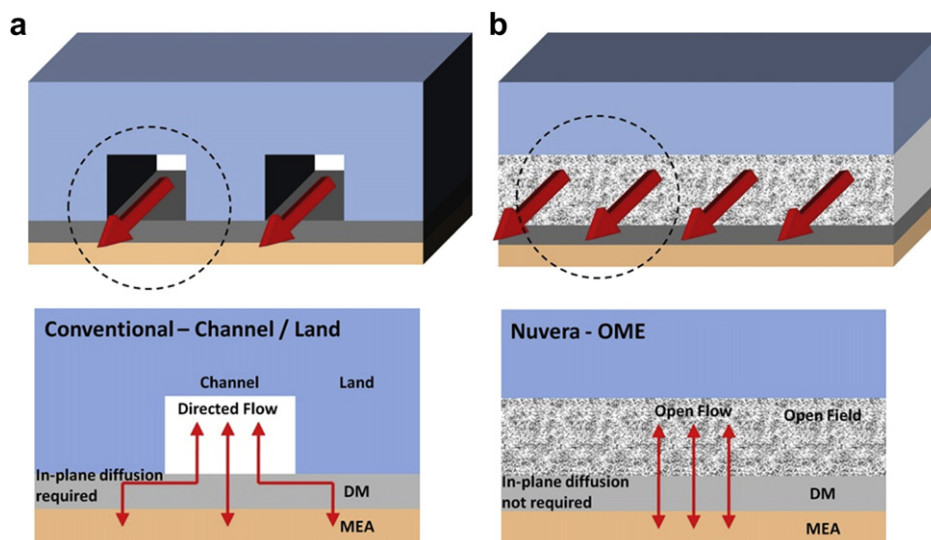
Fig. 1. a) Channel/land, b) open metallic element. (not to scale).

materials and architecture, these conditions cause performance problems due to increased ionic losses, and high mass transport limitation. The maximum power density achieved does not exceed 0.675 W cm^{-2}, and the cell does not operate stably above 1.5 A cm^{-2}. The conditions utilized for this study, with backpressure on both reactant streams, result in better performance throughout the current density range due to enhanced electrode kinetics and mass transport [24–26]. Concurrently, the cell generates 0.9 W cm^{-2}. However, a sharp decrease in performance is still visible at current densities higher than 1.5 A cm^{-2}, and is generally a result of the mass transport limitations. The conventional designs are inadequate in efficient water removal from the cell components resulting in blockage of reactant diffusion into the reaction sites and causing flooding losses. This is visible in Fig. 3, taken with neutron imaging from [27]. Water accumulates under the lands and moves from under the land toward the inner walls of the channel, and therefore retarding the water removal process [27]. The performance curve with heliox at the cathode clearly shows the improvement in mass transport by increasing diffusivity of oxygen into the reaction sites. This performance decrease at the high

current region is a significant problem in terms of obtaining high power density, which is a critical parameter in automotive applications in particular.

The OME design studied here greatly improves the cell performance in the mass limited region while using the same operating conditions. As seen in Fig. 4, at the same conditions (air at the cathode, low humidity, and automotive pressure conditions) the open flow field architecture yields a 25% increase in the limiting current density, mainly through better mass transfer. To the author's knowledge, the 3 A cm^{-2} value is the highest reported limiting current density in the open literature at reasonable operating voltage in air environments. The OME also results in a reduced ohmic resistance, as seen from the mid-current region. The performance curves for both cells are identical up to 0.5 A cm^{-2}, which is expected since they both use the same MEA, and therefore should have the same kinetic behavior. The most important
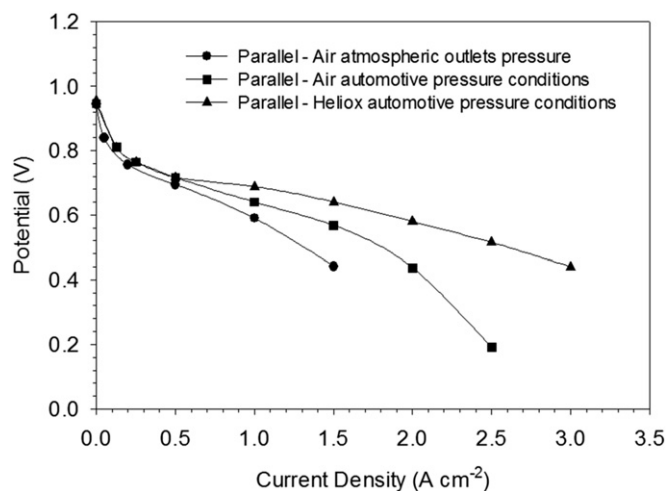

Fig. 2. Parallel flow field performance at 60 °C, under different backpressure and cathode gas dilution. (no backpressure for air, automotive pressure conditions for air, automotive pressure conditions for heliox).
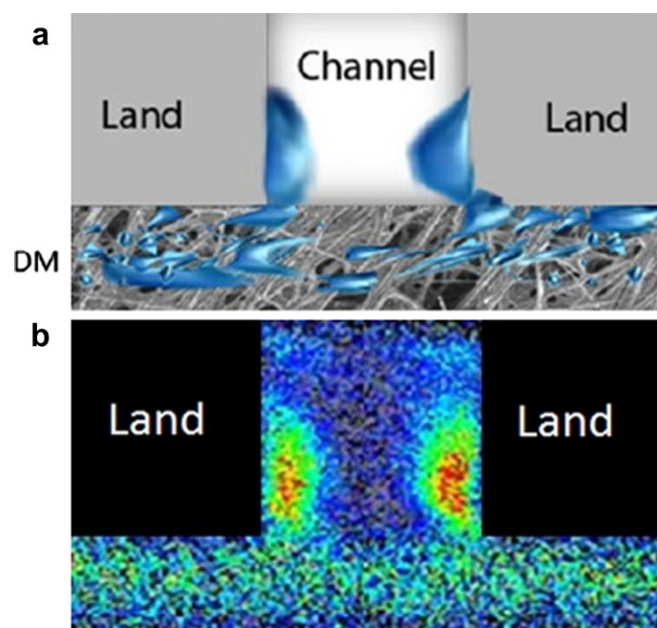

Fig. 3. a) Water buildup in channel and under the lands of a channel/land cell architecture, b) real-time neutron image of water buildup, reproduced from [27].
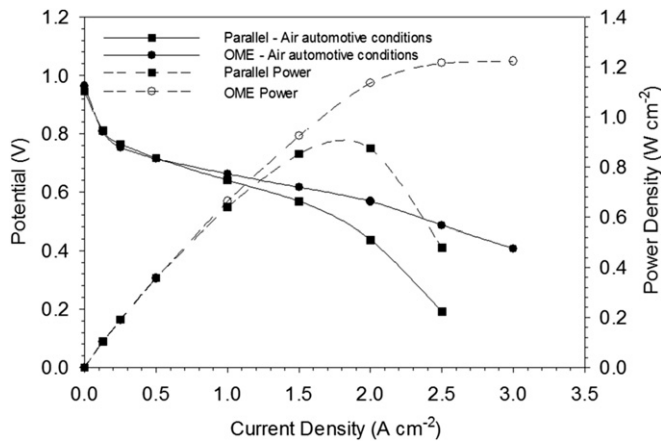
Fig. 4. Performance comparison between OME and parallel flow field at 60 °C, with dry air flow at the cathode using automotive conditions shown in Table 1.
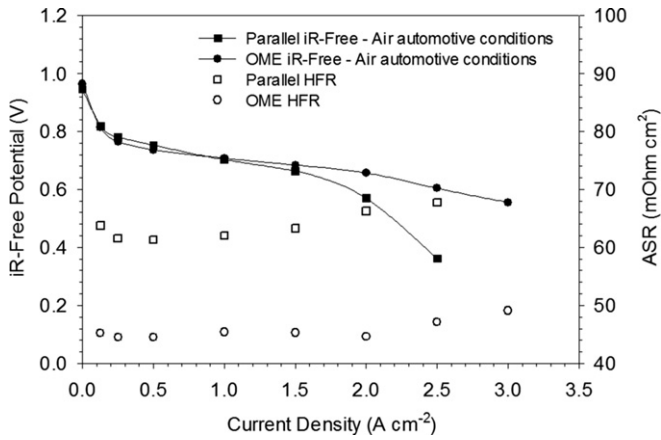

Fig. 5. IR-free performance comparison between OME, and parallel flow field, with respective ASR at 60 °C and air at the cathode, under automotive conditions.

outcome of the boost in performance is seen by comparing power density curves, where the use of OME successfully eliminated the diminishing return of power density at ultra-high currents. As a result a 33% increase in power density is obtained, from 0.9 W cm^{-2} (1.6 W mg^{-1} Pt) with the parallel channel/land architecture to 1.2 W cm^{-2} (2.2 W mg^{-1} Pt) with the OME. This substantial gain in power density enables higher power operation, and therefore greatly decreases the size and cost of stacks for automotive application through less use of expensive catalyst and smaller auxiliary components. Peak power values for both cells are summarized in Table 2.

The performance improvement with the open flow field is further analyzed by means of area specific resistance (ASR) data for both designs. As seen in Fig. 5, the ASR for the open flow field is almost 50% lower than that of the conventional design. The ASR value consists of both the membrane ionic resistance and the contact resistance between the cell components. The lower ASR strongly suggests that more uniform compression, and therefore better contact is achieved with the OME. The iR-free curves of Fig. 5 almost overlap in the low and mid-current density regions of both cells (i.e. up to 1.5 A cm^{-2}) as an indication of vastly similar kinetic and mass transport behavior between the two cases in this current region. However, the sharp performance drop observed with the parallel cell at current densities higher than 1.5 A cm^{-2} is not apparent with the OME. Since the curves are compensated for resistive losses, this enhancement clearly is a result of better mass transport obtained with the OME design.

3.2. Analysis of mass transport region for OME and parallel flow fields

The considerable gain in performance with the use of OME as a flow field is mainly attributed to the mass transport improvements in the high current density region. In order to investigate the difference at high current density, a heliox mixture containing the same mole fraction of oxygen as that of air (21% O$_2$, Bal. He) was fed

Table 2
Peak power of OME and parallel channel/land cells at cell temperature of 60 °C using automotive conditions shown in Table 1.

	OME	Parallel channel/land
Peak power density (W cm^{-2})	1.2	0.9
Peak power per catalyst loading (W mg^{-1} Pt)	2.2	1.6

at the cathode of both cells. At the temperature of 60 °C and pressure conditions up to 180 kPa, oxygen diffusivity in helium gas is 4.1 times higher than in nitrogen, and water vapor diffusivity in helium is 3.8 times higher than in nitrogen [28]. As shown in Fig. 6(a), there is noticeable increase in performance when heliox is introduced in the parallel C/L cell. The limiting current density is increased, and the performance curve is now more linear indicative of less mass transport resistance. When this automotive heliox test on the parallel cell is compared with the automotive air performance of the OME, as seen in Fig. 6(b), a close match is found.
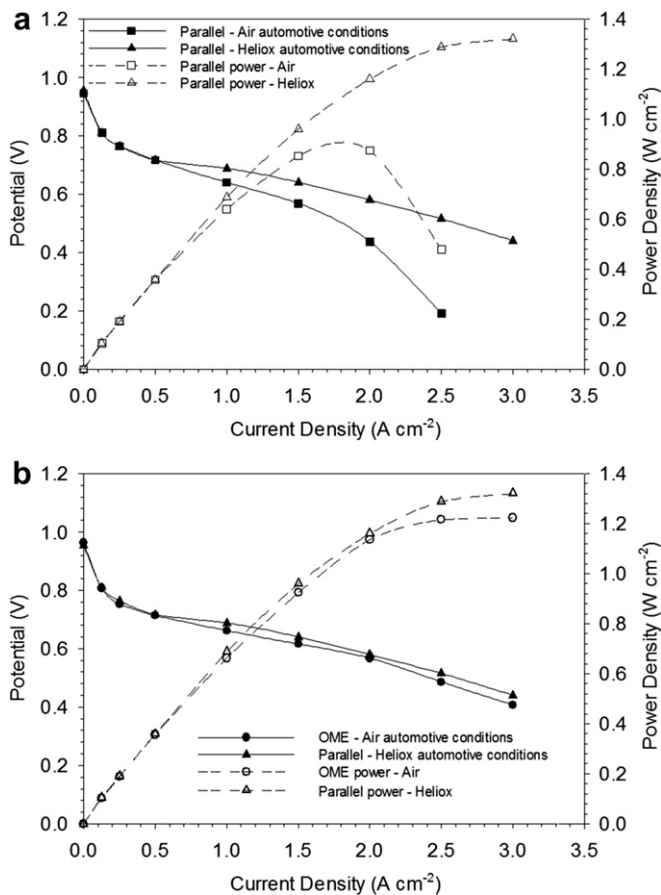

Fig. 6. Effect of heliox mixture on performance at 60 °C with automotive operating conditions: a) effect on parallel cell b) OME air and parallel heliox.
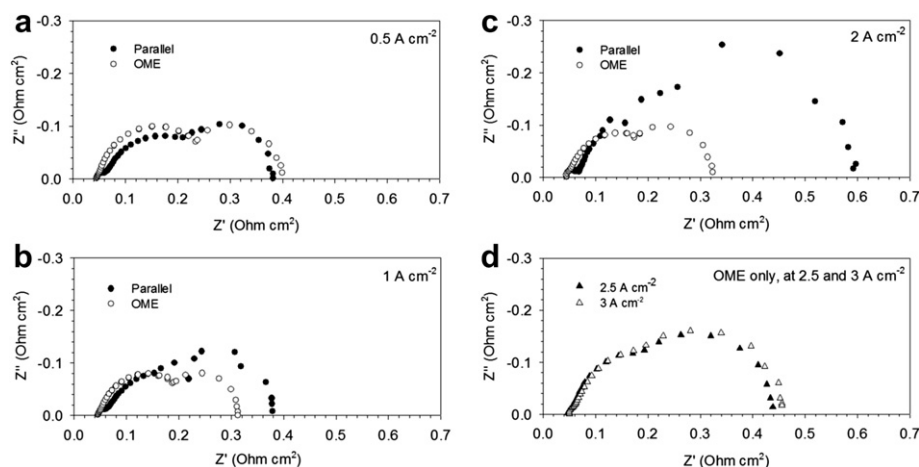
Fig. 7. Nyquist plot for parallel and OME with air flow at the cathode: a) 0.5 A cm^{-2}, b) 1 A cm^{-2}, c) 2 A cm^{-2}, d) OME only at 2.5 and 3 A cm^{-2}.

Complete electrochemical impedance spectroscopy (EIS) data for both cells is shown in Nyquist plots of Fig. 7. Note that air is used as the oxidant in both cases for the EIS data, and Fig. 7(d) is only OME data as it is operating at ultra-high current densities above 2 A cm^{-2}. The smaller low frequency diameter of the semicircle with the OME suggests lower transport resistance compared to conventional parallel design. The Nyquist plots of Fig. 7 were fit to the commonly employed equivalent circuit shown in Fig. 8(a) [29,30]. The medium and low-frequency response arcs are characteristics of cathode charge-transfer and mass-transport processes, and are modeled with a resistor (Rct_Cat) and a finite diffusion Warburg impedance (Ws1) respectively, in series. The double layer capacitance for the cathode is represented with a constant phase element (CPE_Cat). The real axis (Z′) intercept corresponds to the ohmic resistance (Rohmic), which consists of the ionic resistance of the membrane in series with the ohmic resistance of the various layers (catalyst layer, micro porous layer, DM, flow field) and their contact resistances. The ohmic resistance is the same resistance mentioned previously as ASR. Deconvolution of the EIS data into charge transfer and mass transport resistances are shown in Fig. 8(b) and (c), respectively. There is a visible sharp increase in transport resistance with the parallel cell at current densities above 1 A cm^{-2}. The sharp increase is not seen with the OME, and the mass transfer resistance flattens after 1 A cm^{-2}. All these results clearly indicate that the OME design greatly reduces mass transport losses and yields in much higher current and power density.

To understand if further improvement in mass transport can be obtained with the OME, heliox was introduced in the cathode of the OME cell under the same automotive conditions. The heliox test on the OME cell resulted in identical performance to the OME cell operating with air at the cathode, except for the limiting current density, as can be seen in Fig. 9. The fact that the performance of the open flow field with heliox was not better than air, contrary to what was observed for the parallel cell, means that the transport of reactants in the open flow field architecture is not restricted by the diffusion of oxygen to the reaction sites. Also, this indicates that ionomer film resistances at the electrode do not prevent operation at extremely high currents.

However, limiting current density with heliox was only 2 A cm^{-2}, compared to 3 A cm^{-2} with air. From this observation we deduce that a phenomena different than transport limitation is determining the cell performance in OME at high current density with heliox. As shown in Fig. 10, the open flow field cell operating
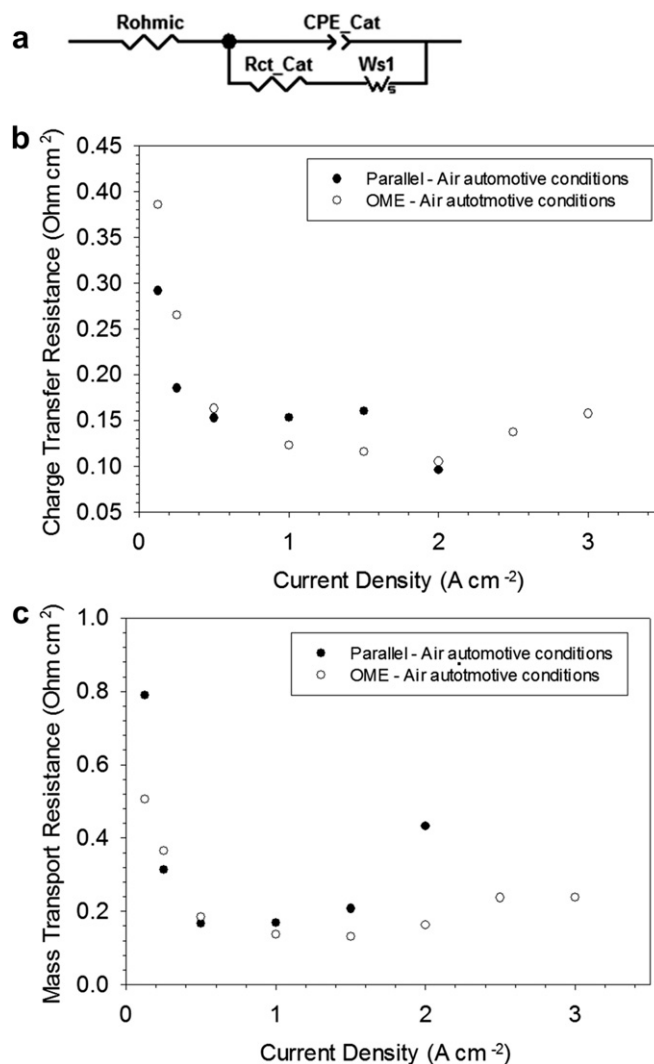

Fig. 8. a) Equivalent circuit employed to fit impedance spectra, b) charge transfer resistance, c) mass transport resistance; with air flow at the cathode using automotive conditions.
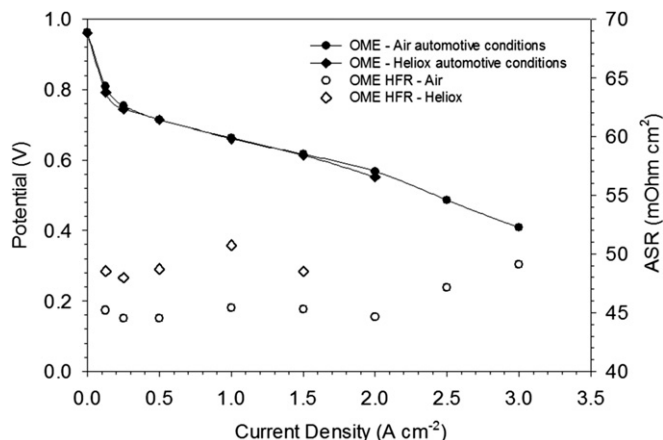
Fig. 9. Effect of heliox mixture on OME performance at 60 °C, using automotive conditions (2 A cm^{-2} is not a stable point with heliox, due to dry-out).
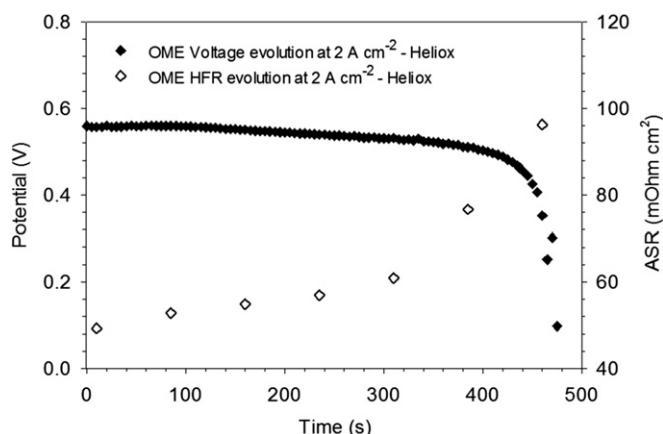

Fig. 10. Voltage and ASR evolution of OME cell at 2 A cm^{-2} with heliox flow at the cathode, and a cell temperature of 60 °C.

with heliox at a constant current density of 2 A cm^{-2} suffered from gradual voltage drop associated with regular increase in ASR. Heliox improves the diffusivity of oxygen and water vapor at the cathode side. In this case, the faster diffusion of water vapor with

heliox caused membrane dry-out by exacerbating the already enhanced diffusion in OME with air flow. In other words, most of the water introduced in the anode side is now removed through the cathode flow with the use of heliox. The results from water balance measurements, as shown in Fig. 11, also confirm this behavior by showing a significant increase in net water drag coefficient at high current density with heliox.

Due to the metallic nature of the OME and corrosion reported in previous metallic flow field studies we considered degradation. We have not observed any visible sign of corrosion after more than 2000 h of operation between various OME cells. This is attributed to the stability of the elements over our range of operating conditions.

4. Conclusion

A performance comparison between the OME architecture fuel cell capable of ultra-high current density and a conventional parallel channel/land architecture was discussed in this work. A stable peak power of 1.2 W cm^{-2} at a current density of 3 A cm^{-2} was generated using the OME architecture, at a cell operating temperature of 60 °C, with low humidity hydrogen at the anode and dry air at the cathode, an improvement of 33% compared to the conventional channel/land design. It was shown that the open flow field architecture improves overall ohmic resistance of the cell through more uniform compression and reduction of contact resistance. The nature of performance improvement through the OME is similar to the boost in performance observed when a heliox mixture is introduced at the cathode of a parallel cell. Mass transport is greatly improved with the OME as the absence of land facilitates and homogenizes water removal, and eliminates the need for in-plane diffusion of the reactants to their specific active electrodes. However, when heliox was used in the OME cell, the combination of the absence of lands and improved water diffusivity in helium limited the current density to 2 A cm^{-2} due to cell dry-out. The ultimate limitation at high current density with OME in air is dry-out due to reduced water retention, and not flooding as commonly observed with conventional C/L flow field. Ionomer film resistances at the electrode do not preclude operation at extremely high currents. Future work will examine in detail the dry-out mechanism at different operating temperatures, and methods for increased water retention with OME.

Acknowledgments

References

[1] DOE hydrogen and fuel cells program record # 11012.
[2] X. Li, I. Sabir, Int. J. Hydrogen Energy 30 (2005) 359–371.
[3] A. Pollegri, P.M. Spaziante, US Patent No. 4, 197,178, 1980.
[4] F. Spurrier, B. Pierce, M. Wright, US Patent No. 4,631,239, 1986.
[5] S. Granata, B. Woodle, US Patent No. 4,684,582, 1987.
[6] D. Jeon, S. Greenway, S. Shimpalee, J. Van Zee, Int. J. Hydrogen Energy 33 (2008) 1052–1066.
[7] G. Hu, J. Fan, S. Chen, Y. Liu, K. Cen, J. Power Sources 136 (2004) 1–9.
[8] L. Wang, H. Liu, J. Power Sources 134 (2004) 185–196.
[9] C. Cavalca, S. Homeyer, E. Walsworth, US Patent No. 5,686,199, 1997.
[10] A. Turhan, K. Heller, J. Brenizer, M.M. Mench, J. Power Sources 160 (2006) 1195–1203.
[11] A. Turhan, K. Heller, J. Brenizer, M.M. Mench, J. Power Sources 180 (2008) 773–783.
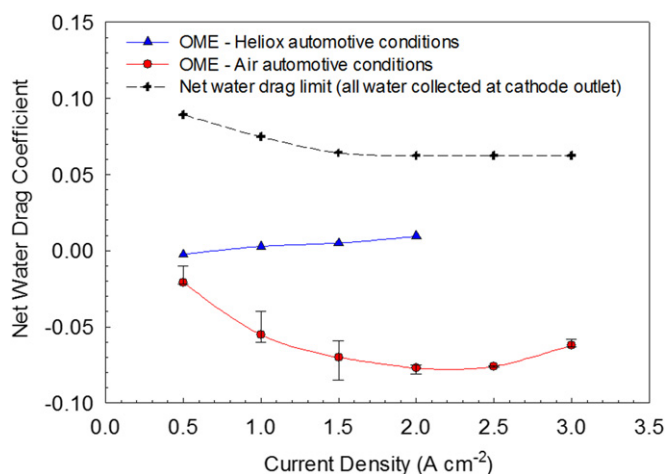[12] K. Cho, M.M. Mench, Int. J. Hydrogen Energy 35 (2010) 12329–12340.

Fig. 11. Measured net water drag coefficient of OME with air, and OME with heliox using automotive conditions. The computed theoretical limit where all the water is collected at the cathode outlet is also plotted.

[13] N. Pekula, K. Heller, P. Chuang, A. Turhan, M.M. Mench, J. Brenizer, K. Unlu, Nucl. Instrum. Methods Phys. Res. 542 (2005) 134–141.
[14] T. Trabold, J. Owejan, D. Jacobson, M. Arif, P. Huffman, Int. J. Heat Mass Transf. 49 (2006) 4712–4720.
[15] S. Goebel, J. Power Sources 196 (2011) 7550–7554.
[16] Y. Lai, P. Rapaport, C. Ji, V. Kumar, J. Power Sources 184 (2008) 120–128.
[17] I. Nitta, T. Hottinen, O. Himanen, M. Mikkola, J. Power Sources 171 (2007) 26–36.
[18] H. Bajpai, M. Khandelwal, E. Kumbur, M.M. Mench, J. Power Sources 195 (2010) 4196–4205.
[19] S. He, M.M. Mench, J. Electrochem. Soc. 153 (2006) 1724–1731.
[20] S. Litster, C. Buie, T. Fabian, J. Eaton, J. Santiago, J. Power Sources 154 (2007) 1049–1058.
[21] J. Yi, J. Yang, C. King, AIChE J. 50 (2004) 2594–2603.
[22] A. Weber, R. Darling, J. Power Sources 168 (2007) 191–199.
[23] L.J. Zheng, A.K. Srouji, A. Turhan, M.M. Mench, J. Electrochem. Soc. 159 (2012) D1.
[24] L. Wang, A. Husar, T. Zhou, H. Liu, Int. J. Hydrogen Energy 28 (2003) 1263–1272.
[25] C. Boyer, S. Gamburzev, A. Appleby, J. Appl. Electrochem. 29 (1999) 1095–1102.
[26] J. Zhang, H. Li, J. Zhang, Electrochem. Soc. Trans. 31 (2009) 65–76.
[27] A. Turhan, S. Kim, M. Hatzell, M.M. Mench, Electrochim. Acta 55 (2010) 2734–2745.
[28] E. Cussler, Diffusion: Mass Transfer in Fluid Systems, second ed., Cambridge University Press, 1997.
[29] D. Malevich, Ela Halliop, A.B. Peppley, G.J. Pharoah, K. Karan, J. Electrochem. Soc. 156 (2009) B216–B224.
[30] N. Fouquet, C. Doulet, C. Nouillant, G. Dauphin-Tanguy, B. Ould-Bouamama, J. Power Sources 159 (2006) 905–913.